# Structure determination of 2,5-difluorophenol by microwave spectroscopy

K.P. Rajappan Nair, Kevin Lengsfeld, Philipp Buschmann, Kenneth Koziol, Brian Esselman, Jens-Uwe Grabow, Ha Vinh Lam Nguyen

# Structure determination of 2,5-difluorophenol by microwave spectroscopy

K. P. Rajappan Nair,[a,b] Kevin G. Lengsfeld,[a] Philipp Buschmann,[a] Kenneth J. Koziol,[c] Brian J. Esselman,[d] Jens-Uwe Grabow,[a] and Ha Vinh Lam Nguyen[c,e*]

[a] Institut für Physikalische Chemie und Elektrochemie, Gottfried-Wilhelm-Leibniz-Universität Hannover, Callinstraße 3A, 30167 Hannover, Germany.

[b] Department of Atomic and Molecular Physics, Manipal Academy of Higher Education, Manipal, 576104, India.

[c] Univ Paris Est Creteil and Université Paris Cité, CNRS, LISA, 94010 Créteil, France.

[d] Department of Chemistry, University of Wisconsin-Madison, Madison, Wisconsin 53706, USA.

[e] Institut Universitaire de France (IUF), 75231 Paris cedex 05, France.

---

* Corresponding author:

Ha Vinh Lam Nguyen, lam.nguyen@lisa.ipsl.fr

## Abstract

The Fourier transform microwave spectrum of 2,5-difluorophenol has been obtained in the centimeter wave range, revealing only one conformer stabilized by an intramolecular interaction where the hydrogen atom of the OH group is in a *syn* orientation to the fluorine atom at the 2-ring position. The heavy atom backbone structure was obtained from the rotational constants of the $^{13}$C and $^{18}$O isotopologues whose spectra were measured in natural abundance. The spectrum of the OD isotopologue obtained by deuterium enrichment was also measured, and the nuclear quadrupole hyperfine structures arising from deuterium were analyzed. The semi-experimental equilibrium structure ($r_e^{SE}$) was determined by correcting the experimental rotational constants with the vibration-rotation interaction constants obtained *via* an anharmonic force field. Quantum chemical calculations at various levels of theory were used to support results from the experiments.



Keywords: microwave spectroscopy, rotational spectroscopy, molecular structure, difluorophenol


## Graphical Abstract

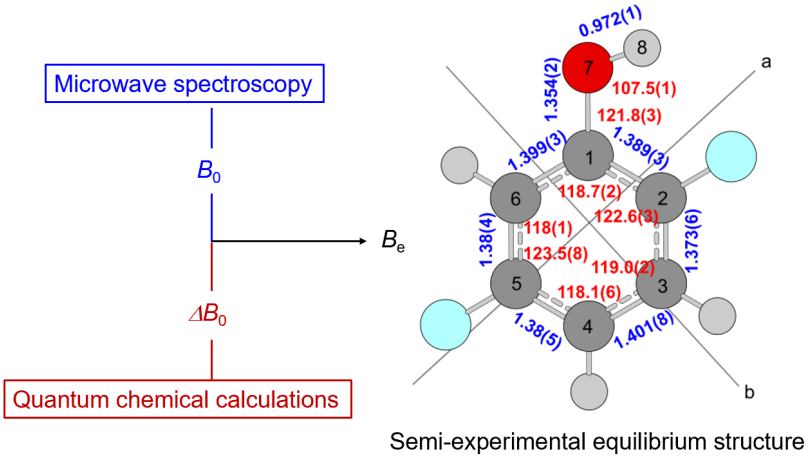


Semi-experimental equilibrium structure

## 1. Introduction

Phenyl containing compounds form a topic of considerable interest due to their existence in a variety of harsh reaction environments such as interstellar medium, Earth's atmosphere, and combustion [1,2]. Regarding the detection of such compounds in the interstellar medium, microwave spectroscopy is consolidating its key role in providing line frequencies helping the detection of, *e.g.*, benzonitrile [3], cyanonaphtalenes [2], benzyne [4], and indene [5]. From a traditional view, the planarity of many phenyl containing molecules, as well as the often intense minor isotopologue transitions, make them interesting to test several structure determination methods and to discover many structural aspects. For example, the microwave structures of coumarin [6], isochroman [7], and 1,4-naphthoquinone [8] revealed a distortion of the perfect π-electron delocalization in benzene due to the presence of a second ring fused to it. In ethynylbenzene, Dreizler, Rudolph, and Hartke reported that the two bond lengths are larger and the bond angle is smaller at the substitution position of the phenyl ring [9]. This has been further elaborated in recent years by the template model [10].

Fluorinated phenyl containing molecules have been studied in the early development of microwave spectroscopy, with the pioneer work of McCulloh and Pollnow on fluorobenzene in 1954 [11], followed by its structure determination first by Bak et al. in 1957 [12] then by Nygaard et al. in 1968 [13]. Continuing with the fluorophenol family, 2-fluorophenol was studied by Datta et al. in 1985 [14], and was reinvestigated by Bell et al. together with 3-fluorophenol [15]. Bell et al. concluded that two planar conformers of 3-fluorophenol with a *syn* and an *anti* orientation of the OH hydrogen relative to the fluorine atom could be detected in the microwave spectrum under supersonic jet conditions, but only the *syn* conformer of 2-fluorophenol was observed [15]. Previous results on 2,3-difluorophenol (23DFP) [16] and 2,4-difluorophenol (24DFP) [17,18] confirm that also in these two fluorophenol derivatives, only the *syn* conformer is present in the jet-cooled spectrum [19]. These observations and previous investigations of 2-fluorophenol indicate that only one conformer of the 2,5-isomer of difluorophenol (25DFP, see Figure 1) will likely be observed in the jet-cooled conditions. Therefore, we continued our systematic investigation with 25DFP to test this assertion.

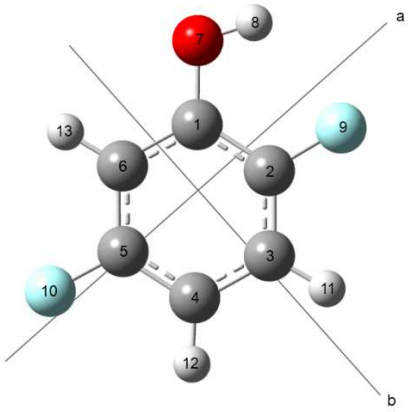


**Figure 1:** The molecular structure of *syn*-25DFP optimized at the MP2/6-311++G(2d,2p) level of theory in the principal axis system. Hydrogen atoms are white; carbon atoms gray; fluorine atoms light blue; and the oxygen atom is red.

The use of pulsed supersonic expansion in combination with Fourier transform microwave (FTMW) spectroscopy has significantly improved both the accuracy and the sensitivity of this spectroscopic method [20]. This enables the observation of minor isotopologues such as $^{13}$C and $^{18}$O in natural abundance, leading to molecular structure determinations with precise information on bond lengths and angles. In the present investigation of 25DFP, our goal is to answer the question about the existence of only the *syn* conformer in the jet, but also to determine its structure for a comparison with those of 23DFP and 24DFP. Structural parameters of a molecule, especially bond lengths and bond angles, are crucial to access a comprehensive view of chemical bonds. Explaining their changes in terms of conjugation, non-covalent interactions, hybridization, and resonance have been pursued to understand chemical bonds. The FTMW technique allows the determination of rotational constants by nine or more significant digits, enabling the detection of factors which influence small changes in bond lengths and angles, such as substitution at the benzene ring [6-8].

Determining the $r_s$ and $r_0$ structures of a molecule by applying directly the rotational constants determined from its microwave spectra without any correction is frequently seen in the microwave spectroscopic community, as having been performed in our previous studies on 23DFP and 24DFP. The most significant drawback of this simple method is that structures obtained from geometry optimizations are at the equilibrium ($r_e$) and cannot be compared directly with the $r_s$ or

$r_0$ structures which are determined using rotational constants of the vibrational ground state. With growing computational capabilities in the last decade, the semi-experimental equilibrium $r_e^{SE}$ structure has become a good choice to overcome this problem. It has been frequently applied on experimental data with anharmonic corrections at high level calculations by theoretical groups [21-33]. This method steps beyond the traditional Kraitchman analysis and enables the possibility to compare bond lengths and bond angles between different molecules. In the present paper, we recommend a cost-efficient method for experimental microwave spectroscopic labs to attain reasonably good $r_e^{SE}$ structures. We applied it on 23DFP, 24DFP, and 25DFP, and were subsequently able to compare directly the geometry parameters of these three isomers without any vibrational effect.

## 2. Quantum chemical calculations

To predict the dependence of the potential energy on the O-H rotation, the dihedral angle $\varphi = \angle(C_2,C_1,O_7,H_8)$ was varied in 10° steps while all other geometry parameters were optimized at the MP2/6-311++G(2d,2p) level of theory. Due to symmetry, a rotation of 180° was sufficient. We found a two-fold potential as illustrated in Figure 2, which was drawn using the Fourier coefficients shown in Table S-1 in the Supplementary Materials obtained from parameterizing the energy points. The potential energy curve displayed two minima at $\alpha = 0°$ (*syn*) and 180° (*anti*), with an energy difference of 12.35 kJ/mol and a $V_2$ term of 7.85 kJ/mol (656 $cm^{-1}$) being the necessary energy to convert the *anti*-conformer into the *syn* one (see Table S-1). According to Ruoff et al. [34], during the expansion in a pulsed supersonic jet, conformers that are separated by a barrier of 400 $cm^{-1}$ or more do not relax to the more stable form. However, from our experiences on 23DFP and 24DFP where the experiments were performed with the same instrument, the *anti*-conformer is too high in energy before the supersonic expansion and not observable under the measurement conditions due to its low initial population. For comparison, the energy difference and the $V_2$ term are 10.72/7.57 kJ/mol and 11.45/6.40 kJ/mol for 23DFP and 24DFP, respectively. The H-F hydrogen bond is clearly the reason for the stability of the *syn* form, which has been also found in 2-fluorophenol [14,15] and 24DFP [17,18]. As expected, we only observed *syn*-25DFP in the microwave spectrum. Therefore, our quantum chemical calculations focus on this conformer.

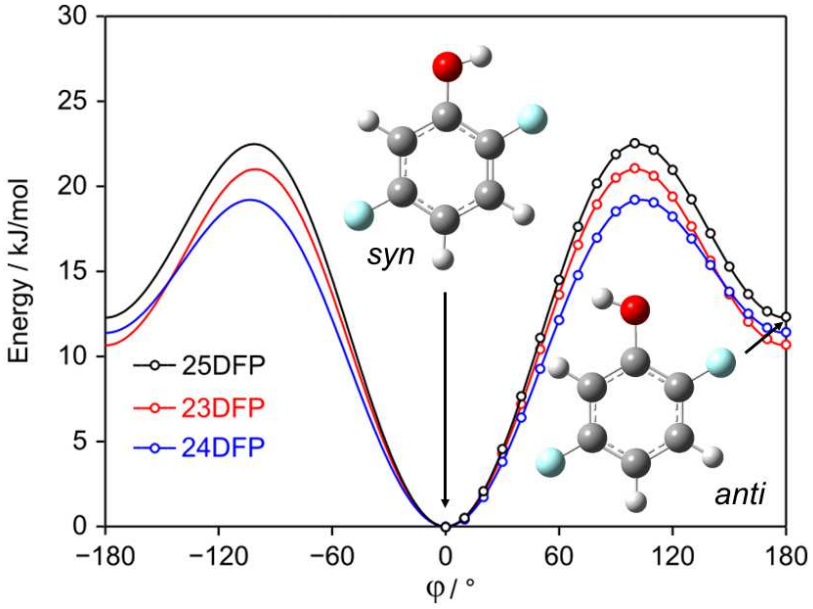


**Figure 2:** The potential energy curve of 25DFP (black line) obtained by rotating the O–H bond. Calculations were carried out at the MP2/6-311++G(2d,2p) level of theory by varying the dihedral angle $\varphi = \angle(C_2,C_1,O_7,H_8)$ in 10° steps. The energies are given relative to the lowest energy conformation with $E_{min}$ = −504.9322318 Hartree. For comparison, the corresponding curves of 23DFP (red) and 24DFP (blue) are also illustrated.

Full geometry optimizations of *syn*-25DFP were first carried out with the second order Møller-Plesset perturbation theory MP2 [35] and density functional theory B3LYP [36,37] methods in combination with Pople's 6-311++G(2d,2p) basis set [38] using the *Gaussian* 16 program package [39] with "verytight" convergence criteria and an "ultrafine" integration grid. These two levels have been used to optimize the structures of 23DFP [16] and 24DFP [17]. Table 1 presents the results of these calculations and the optimized geometry is displayed in Figure 1. All atoms are coplanar including the OH hydrogen atom due to the presence of a hydrogen bond with the fluorine atom at the 2-position of the phenyl ring. The molecule is calculated to be a $C_s$ prolate top with comparably large dipole moment components along the *a*- and the *b*-axes ($\mu_{a,MP2}$ = 0.98 D and $\mu_{b,MP2}$ = 1.00 D). The microwave spectrum is expected to display intense *a*- and *b*-type bands. The Cartesian coordinates in the principal axes of inertia are given in the Supplementary Materials in Table S-2. Harmonic frequency calculations at the same levels of theory were performed to confirm the geometry to be a stable conformer and to access zero-point

energy corrections. Subsequent anharmonic frequency calculations yielded the ground state rotational constants and centrifugal distortion constants. Additional magnetic calculations (nmr=susceptibility) were performed to obtain the rotational *g*-tensors to determine the electron mass corrections to the rotational constants.

**Table 1.** Experimental and quantum chemically predicted rotational constants *A*, *B*, *C* and dipole moment components $\mu$ of *syn*-2,5-difluorophenol as obtained at the MP2/6-311++G(2d,2p) and B3LYP-D3BJ/6-311++G(2d,2p) levels of theory. Centrifugal distortion constants were calculated at the B3LYP-D3/6-311+G(2d,p) level used for the structure determination (see section 4.2). The experimental data are also given.

| Par.[a] | Unit | MP2 | B3LYP | Experiment |
|---|---|---|---|---|
| $A_0$ | MHz | 3164.3 | 3178.7 | 3161.81447(10) |
| $B_0$ | MHz | 1278.2 | 1282.2 | 1283.667636(37) |
| $C_0$ | MHz | 910.4 | 913.6 | 913.026450(28) |
| $D_J$ | kHz | | 0.0213 | 0.02123(16) |
| $D_{JK}$ | kHz | | 0.0859 | 0.08953(75) |
| $D_K$ | kHz | | 0.4323 | 0.4451(49) |
| $d_1$ | kHz | | –0.00727 | –0.00773(10) |
| $d_2$ | kHz | | –0.00174 | –0.001778(49) |
| $\lvert\mu_a\rvert$ | D | 1.0 | 1.0 | - |
| $\lvert\mu_b\rvert$ | D | 0.9 | 0.9 | - |
| $\lvert\mu_c\rvert$ | D | 0.0 | 0.0 | - |
| $\mu_{total}$ | D | 1.4 | 1.4 | - |
| *rms*[b] | kHz | | | 0.9 |
| *N*[c] | | | | 66 |

[a] All parameters refer to the principal axis system using an S-reduced Hamiltonian in the $I^r$ representation. Standard errors in parentheses are in the units of the last digits. [b] Root-mean-square deviation of the fit. [c] Number of fitted lines.

Afterwards, several methods in addition to MP2 and B3LYP were tested for benchmarking purpose, including Truhlar's M06-2X [40] and Head-Gordon's ωB97X-D [41] as well as the Perdew-Burke-Ernzerhof [42] and Minnesota MN15 [43] methods in combination with different Pople [38] and Dunning [44] basis sets. For B3LYP calculations, Grimme's dispersion corrections with the zero- (D3) [45] or Becke-Johnson (BJ) damping [46] were applied, but also the version with the Coulomb-attenuating method (CAM) [47]. The results are given in Table S-3. For

benchmarking purposes, the basis set variation was also done for 23DFP and 24DFP to figure out the method-basis set combination most suitable to guide the assignment of difluorophenol derivatives (see also Table S-3).

## 3. Microwave spectroscopy

### 3.1. Experimental details

A sample of 25DFP was purchased from Sigma-Aldrich, Germany, and used without further purification. Rotational transitions were recorded using two molecular jet Fourier transform microwave spectrometers with coaxially oriented beam-resonator arrangement (COBRA) operating from 2 to 26 GHz [48], one in Aachen (now in Paris, France) and one in Hannover, Germany. The substance was placed in a small reservoir at the nozzle orifice. Neon or helium as carrier gas was flown over the sample at stagnation pressures of 1-2 bar, and the 25DFP-rare gas mixture was expanded into the resonator chamber. The experimental accuracy is estimated to be 2 kHz. Lines of the $^{13}C$ and $^{18}O$-isotopologues were measured in natural abundance. For the OD deuterated species, an enriched sample was prepared by D-exchange with heavy water. A mixture of the sample and $D_2O$ was stirred in an UV bath for a few hours. Due to the nuclear spin $I = 1$ of deuterium, transitions of this species show hyperfine splittings arising from the nuclear quadrupole coupling to the end-over-end rotation. Figure 3 depicts a typical spectrum with the deuterium hyperfine structure. The spectra of the deuterated species were more intense than many of the OH difluorophenol species.

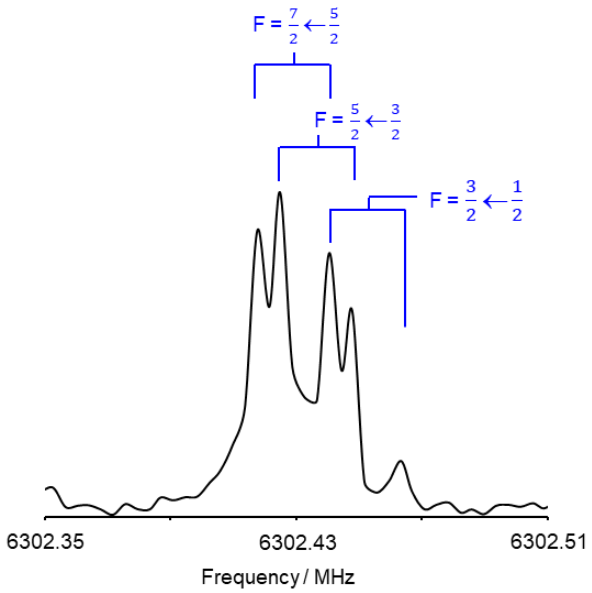


**Figure 3:** A typical spectrum of the $J''_{K_a''K_c''} - J'_{K_a'K_c'} = 3_{03} - 2_{02}$ rotational transition with its deuterium hyperfine structure of the OD species of 25DFP. The Doppler doublets are marked by brackets. The quadrupole hyperfine components $F = J + I$ are given.

### 3.2. Spectral assignment and fits

Preliminary rotational constants were taken from the $B_e$ values calculated at the MP2/6-311++G(2d,2p) level of theory and used to search for *a*-type transitions with low *J*-quantum numbers. They were well-predicted and could be rapidly identified. Subsequently, other *a*-type *R*-branch and also *b*-type *R*- and *Q*-branch lines were measured. Finally, 66 lines were fitted with *spfit* [49] using a quartic centrifugally distorted rotor S-reduced Hamiltonian to an rms deviation of 0.9 kHz, within the experimental accuracy. All quartic centrifugal distortion constants were accurately determined for the main isotopologue. The obtained spectroscopic parameters are collected in Table 1. The fitted frequencies are listed in Table S-4 in the Supplementary Materials along with the residuals obtained with *spfit*.

Using the MP2/6-311++G(2d,2p) predicted structure of the parent species, estimates of the rotational constants of the six inequivalent $^{13}C$, the $^{18}O$, and the OD-isotopologues were calculated by adjusting the mass of the substituted atom. The theoretical frequencies of the searched isotopologue were corrected with the differences between the experimental frequencies and the

frequencies predicted with the MP2/6-311++G(2d,2p) $B_e$ constants of the parent species. The lines were quickly found for all $^{13}C$ isotopologues in their natural abundance of 1% as well as for the enriched OD-species prepared as described in section 3.1. For the $^{18}O$-isotopologue with a lower natural abundance of 0.2 %, the search was more intense and small scans with more co-added decays at each scan step were needed. The determined parameters of these isotopologues are also reported in Tables 2 and 3. The measured transition frequencies and residuals along with the quantum assignments are given in Tables S-4 and S-5 in the Supplementary Materials.

**Table 2.** Determined parameters of the $^{13}C$ and $^{18}O$ isotopologues of 25DFP obtained using a semi-rigid rotor Hamiltonian model. Atoms are numbered according to Figure 1.

| Par.[a] | Unit | $^{13}C(1)$ | $^{13}C(2)$ | $^{13}C(3)$ | $^{13}C(4)$ | $^{13}C(5)$ | $^{13}C(6)$ | $^{18}O(7)$ |
|---|---|---|---|---|---|---|---|---|
| $A_0$ | MHz | 3149.96896(11) | 3155.95784(19) | 3112.61166(56) | 3129.19128(14) | 3161.87322(13) | 3138.78672(28) | 3043.73457(28) |
| $B_0$ | MHz | 1282.105412(83) | 1279.83412(10) | 1283.58658(30) | 1279.113129(72) | 1275.810267(67) | 1282.29922(15) | 1266.75900(12) |
| $C_0$ | MHz | 911.247764(47) | 910.599351(72) | 908.83753(21) | 907.993931(52) | 909.049786(49) | 910.40869(11) | 894.507006(69) |
| $D_J$ | kHz | 0.02267(59) | 0.0238(10) | 0.0231(23) | 0.02277(73) | 0.02225(66) | 0.0216(15) | 0.0210(15) |
| $D_{JK}$ | kHz | 0.0768(54) | 0.0748(91) | [0.089528] | 0.0721(65) | 0.0856(60) | 0.0755(13) | 0.085(18) |
| $D_K$ | kHz | [0.445149] | [0.445149] | [0.445149] | [0.445149] | [0.445149] | [0.445149] | [0.445149] |
| $d_1$ | kHz | –0.00694(38) | –0.00723(65) | [–0.007728] | –0.00700(49) | –0.00694(45) | –0.00544(96) | –0.00596(86) |
| $d_2$ | kHz | [–0.001778] | [–0.001778] | [–0.001778] | [–0.001778] | [–0.001778] | [–0.001778] | [–0.001778] |
| *rms*[b] | kHz | 0.6 | 1.0 | 3.1 | 0.7 | 0.7 | 1.5 | 0.9 |
| $N$[c] | | 40 | 40 | 40 | 40 | 40 | 41 | 35 |

[a] All parameters refer to the principal axis system using an S-reduced Hamiltonian in the $I^r$ representation. Standard errors in parentheses are in the units of the last digits. Parameters in brackets given with values without errors are fixed to the values of the parent species fit (see Table 1).

[b] Root-mean-square deviation of the fit.

[c] Number of independent transitions.

**Table 3.** Determined rotational constants, centrifugal distortion constants, and quadrupole coupling constants of the OD-isotopologue of 25DFP.

| Par.[a] | Unit | OD | B3LYP[b] |
|---|---|---|---|
| $A_0$ | MHz | 3125.00912(43) | 3151.507 |
| $B_0$ | MHz | 1263.58613(11) | 1276.183 |
| $C_0$ | MHz | 899.812664(44) | 908.362 |
| $D_J$ | kHz | 0.02205(73) | 0.02123 |
| $D_{JK}$ | kHz | [0.08606][c] | 0.08606 |
| $D_K$ | kHz | [0.46172][c] | 0.46172 |
| $d_1$ | kHz | –0.00768(43) | –0.00721 |
| $d_2$ | kHz | [–0.00172][c] | –0.00172 |
| $\chi_{aa}$ | MHz | 0.2421(86) | 0.2406 |
| $\chi_{bb}$[d] | MHz | –0.079(11) | –0.0673 |
| $\chi_{cc}$[d] | MHz | –0.164(23) | –0.1733 |
| *rms*[e] | kHz | 1.5 | |
| $N$[f] | | 37/47 | |

[a] All parameters refer to the principal axis system. Watson's S reduction and $I^r$ representation were used.

[b] Ground state rotational constants and centrifugal distortion constants calculated at the B3LYP-D3BJ/6-311++G(2d,2p) level of theory obtained from anharmonic frequency calculations.

[c] Not well-determined. Fixed to the calculated values.

[d] Derived from the fitted parameters $\chi_{aa}$ and $\chi_{bb} - \chi_{cc}$ = 0.0228(32) MHz.

[e] Root-mean-square deviation of the fit.

[f] Number of rotational transitions and number of resolved hyperfine components. Only for a few transitions, the hyperfine structure is resolved (see Table S-5).

## 4. Structure determination

### 4.1. The $r_s$ and $r_0$ structure

The structure of 25DFP could be determined using the rotational constants of the main species as well as those of the $^{13}C$, $^{18}O$, and OD-isotopologues with Kraitchman's equation [50] as implemented in the programs *KRA* and *EVAL* [51]. The signs of the atom coordinates were taken from the optimized geometry as given in Table S-2 and the uncertainties were calculated with Costain's rule [52]. The experimentally determined atom coordinates are reported in Table 4, the bond angles and bond lengths in Table 5.

**Table 4**. Experimental atom positions of *syn*-25DFP. $r_s$ refers to the substitution structure obtained with Kraitchman's equations using directly the experimentally deduced rotational constants. $r_s^{SE}$ and $r_e^{SE}$ are the semi-experimental equilibrium structures where the experimental rotational constants are corrected with anharmonic cubic force field before inputting in either the program *KRA* or the program *STRFIT*, respectively. Anharmonic corrections were obtained at the B3LYP-D3/6-311+G(2d,p) level. All *c*-coordinates were set to zero due to planarity. The $r_e$ equilibrium atom positions calculated at the B3LYP-D3/6-311+G(2d,p) level are also given for comparison. Note that the *b*-coordinate of the C(5) atom, lying close to the *a*-axis (see Figure 1), could not be well-determined.

| | $r_s$ | | $r_s^{SE}$ | | $r_0$ | | $r_e^{SE}$ | | $r_e$ | |
|---|---|---|---|---|---|---|---|---|---|---|
| | *a*/Å | *b*/Å | *a*/Å | *b*/Å | *a*/Å | *b*/Å | *a*/Å | *b*/Å | *a*/Å | *b*/Å |
| C(1) | 0. 6931(22) | –0.7777(19) | 0.7008(21) | –0.7803(20) | 0.6932(69) | –0.7788(59) | 0.6972(69) | –0.7816(59) | 0.70011 | –0.78470 |
| C(2) | 1.0875(14) | 0.5469(24) | 1.0905(14) | 0.5527(28) | 1.0876(39) | 0.5481(53) | 1.0881(39) | 0.5530(52) | 1.09042 | 0.55298 |
| C(3) | 0.1565(96) | 1.59305(94) | 0.1876(80) | 1.58763(95) | 0.164(17) | 1.5932(26) | 0.187(17) | 1.5872(26) | 0.18155 | 1.58875 |
| C(4) | –1.1823(13) | 1.2975(12) | –1.1823(13) | 1.2943(12) | –1.1820(38) | 1.2983(34) | –1.1770(38) | 1.2968(34) | –1.18047 | 1.29801 |
| C(5) | –1.56048(96) | –0.056(27) | –1.56280(96) | –0.031(48) | –1.5596(25) | –0.0342(26) | –1.5575(24) | –0.0319(26) | –1.56288 | –0.03229 |
| C(6) | –0.6475(23) | –1.0859(14) | –0.6655(23) | –1.0809(14) | –0.6466(67) | –1.0871(41) | –0.6533(66) | –1.0842(41) | –0.65877 | –1.07981 |
| O(7) | 1.61020(93) | –1.79254(84) | 1.60483(93) | –1.78861(84) | 1.6101(15) | –1.7927(13) | 1.6037(15) | –1.7890(13) | 1.60348 | –1.79895 |
| H(8) | 2.49202(60) | –1.3893(11) | 2.48982(60) | –1.3872(11) | 2.4924(19) | –1.3907(33) | 2.4883(19) | –1.3881(33) | 2.49624 | –1.42932 |
| F(9)[a] | | | | | 2.4304(77) | 0.8094(65) | 2.4145(78) | 0.8014(63) | 2.42964 | 0.80859 |
| F(10)[a] | | | | | –2.8780(28) | –0.3365(27) | –2.8767(27) | –0.3305(27) | –2.88238 | –0.32965 |
| H(11)[a] | | | | | –1.957(27) | 2.0971(26) | –1.928(27) | 2.081(27) | –1.92867 | 2.07801 |
| H(12)[a] | | | | | 0.530(31) | 2.644(33) | 0.552(31) | 2.610(34) | 0.54162 | 2.60910 |
| H(13)[a] | | | | | –0.991(18) | –2.145(33) | –0.994(18) | –2.115(34) | –0.99585 | –2.10713 |

[a] The two CF and three CH bond lengths were varied in the fitting but constrained to be the same.

**Table 5**. Bond lengths and bond angles deduced from the $r_s$, $r_0$, $r_s^{SE}$, $r_e^{SE}$, and $r_e$ structures of *syn*-25DFP given in Table 4. The OH bond length and C1–O–H bond angle are bold to highlight that only for these two parameters, differences between the $r_e^{SE}$ and the $r_e$ structures are observed.

| | $r_s$ | $r_0$ | $r_s^{SE}$ | $r_e^{SE}$ | $r_e$ |
|---|---|---|---|---|---|
| C1–C2 | 1.3821(33) | 1.3843(89) | 1.3888(33) | 1.3906(89) | 1.3935 |
| C2–C3 | 1.4004(68) | 1.395(15) | 1.3734(58) | 1.372(15) | 1.3780 |
| C3–C4 | 1.3710(94) | 1.378(19) | 1.4009(79) | 1.394(19) | 1.3927 |
| C4–C5 | 1.406(26) | 1.3850(54) | 1.379(46) | 1.3821(55) | 1.3842 |
| C5–C6 | 1.376(20) | 1.3936(63) | 1.381(36) | 1.3875(63) | 1.3837 |
| C6–C1 | 1.3756(31) | | 1.3990(31) | | 1.3906 |
| C1–O7 | 1.3679(22) | 1.3670(45) | 1.3542(22) | 1.3553(46) | 1.3582 |
| O–H | 0.9697(12) | 0.9696(27) | 0.9717(12) | **0.9712(27)** | **0.9663** |
| C–H | | 1.113(38) | | 1.086(38) | 1.0812 |
| C–F | | 1.368(11) | | 1.349(11) | 1.3526 |
| C1–O–H | 107.53(13) | 107.63(36) | 107.48(13) | **107.60(36)** | **109.20** |
| C2–C1–C6 | 119.53(17) | | 118.70(17) | | 118.52 |
| C2–C1–O | 121.32(17) | 121.33(51) | 121.83(17) | 121.69(52) | 122.043 |
| C6–C1–O | 119.15(16) | | 119.47(16) | | 119.44 |
| C1–C2–C3 | 121.75(32) | 121.98(58) | 122.60(29) | 122.61(57) | 122.47 |
| C2–C3–C4 | 119.22(24) | 119.11(27) | 119.01(22) | 119.05(28) | 119.22 |
| C3–C4–C5 | 118.06(32) | 118.18(25) | 118.10(56) | 118.00(25) | 118.09 |
| C4–C5–C6 | 122.83(46) | 123.25(30) | 123.45(75) | 123.34(30) | 123.16 |
| C5–C6–C1 | 118.62(75) | | 118.1(13) | | 118.54 |

Since only rotational constants of the $^{13}C$, $^{18}O$, and OD-isotopologues are available, we could not determine the complete structure of 25DFP because information about the atom locations of the two fluorine atoms and the three CH hydrogen atoms is lacking. However, their coordinates can be taken from quantum chemical calculations to input in the program *STRFIT* [51,53] for a least-squares fit which yields the $r_0$ structure. We allowed all five atom locations to vary in the fitting, but the CF bond lengths as well as the CH lengths are constrained to be the same (average values). Results of the $r_0$ structure are also displayed in Tables 4 and 5.

### 4.2. The semi-experimental equilibrium $r_e^{SE}$ structures

The main point of the $r_e^{SE}$ structure determination is that the experimentally determined $A_{0,exp.}$, $B_{0,exp.}$, $C_{0,exp.}$ rotational constants are corrected by the differences between the equilibrium $A_e$, $B_e$, $C_e$ rotational constants predicted from geometry optimizations and the ground state $A_{0,calc.}$, $B_{0,calc.}$, $C_{0,calc.}$ obtained from anharmonic frequency calculations. The two main contributions of the difference between the $B_0$ and $B_e$ constants are the vibration-rotation interactions and the electron mass corrections as shown in Equation 1.

$$B_e = B_0 + \frac{1}{2}\sum \alpha_i - \eta g^{bb} B \qquad (1)$$

To a first approximation, the vibration-rotation interaction is one half the sum of the $\alpha$ values for each of the fundamental vibrations. The electron mass calculation is calculated from the electron-proton mass ratio ($\eta$), the rotational $\boldsymbol{g}$ tensor, and the corresponding rotational constant. These corrections obtained from anharmonic frequency and magnetic calculations of each isotopologue are applied to all of the rotational constants prior to structure determination. The corrected experimental rotational constants $A_e^{SE}$, $B_e^{SE}$, $C_e^{SE}$ are then used to determine the semi-experimental equilibrium $r_e^{SE}$ structures, either with the program *KRA* ($r_s^{SE}$ structure) or with the program *STRFIT* ($r_e^{SE}$ structure).

The quality and importance of the corrections to the rotational constants for a planar molecule like 25DFP can be assessed by their impact on the inertial defects ($\Delta_i$). The equilibrium inertial defect for a planar molecule must be zero, whereas the inertial defect determined from the experimentally observed rotational constants will deviate from zero due to the aforementioned vibration-rotation interactions and electron mass distribution. Table 6 provides the inertial defect values for each isotopologue calculated from the experimental rotational constants, with vibration-rotation interaction corrections, and with both vibration-rotation interaction and electron mass corrections. As expected, the vibration-rotation interaction corrections result is a substantial decrease in the magnitude of the inertial defect (by about 50%). A further reduction of magnitude of the inertial defect is observed with the application of the electron mass corrections. This is consistent with previous works using coupled-cluster or DFT corrections to the vibration-rotation interaction and the electron mass correction [28,54]. While the DFT calculations employed in this work provide an expedient alternative to more expensive coupled cluster calculations, the resulting

equilibrium inertial defects ($\Delta_{i,e}$) in Table 6 are about three times larger than those obtained for pyridazine both with and without electron mass corrections [55]. This is evidence that further improvement in the structure would be possible by increasing the level of theory for the anharmonic frequency calculation. The large size of 25DFP, however, makes such a calculation daunting. We are confident that the corrections employed in this work will provide a substantial improvement over a more traditional $r_0$ or $r_s$ structure.

**Table 6**. Inertial defects ($\Delta_i$) of 25DFP isotopologues.

| Isotopologue | $\Delta_{i,0}$ (uÅ$^2$) | $\Delta_{i,e}$ (uÅ$^2$)[a] | $\Delta_{i,e}$ (uÅ$^2$) |
|---|---|---|---|
| $^{12}$C | –0.01689 | –0.00863 | 0.00382 |
| $^{13}$C(1) | –0.01725 | –0.00884 | 0.00359 |
| $^{13}$C(2) | –0.01742 | –0.00884 | 0.00359 |
| $^{13}$C(3) | –0.01717 | –0.00902 | 0.00337 |
| $^{13}$C(4) | –0.01724 | –0.00889 | 0.00356 |
| $^{13}$C(5) | –0.01721 | –0.00876 | 0.00369 |
| $^{13}$C(6) | –0.01811 | –0.00897 | 0.00345 |
| OD | –0.01297 | –0.00904 | 0.00340 |
| $^{18}$O(7) | –0.02791 | –0.00827 | 0.00424 |
| Average ($\bar{x}$) | –0.0180 | –0.00881 | 0.00363 |
| Std. Dev. (s) | 0.0040 | 0.00024 | 0.00027 |

[a] Vibration-rotational correction only.

We first performed anharmonic corrections at two levels of theory, B3LYP-D3/6-311+G(2d,p) and B3LYP-D3/aug-cc-pVTZ. The two $r_e^{SE}$ structures of 25DFP obtained at the B3LYP-D3/6-311+G(2d,p) level are reported in Tables 5 and 6; those obtained at the B3LYP-D3/aug-cc-pVTZ level in Table S-6 in the Supplementary Materials. The corrected rotational constants at the B3LYP-D3/6-311+G(2d,p) level are in Table S-7. For comparison, we also determined the $r_e^{SE}$ structures of 23DFP and 24DFP with the results given in Tables S-8 and S-9, as well as illustrated in Figure 4. It can be seen in Figure 4 that the structure determination of 23DFP is very problematic since the C(1) and C(3) atoms both lay quite close to the *a*-axis and the C(2) and C(5) atoms both lay quite close to the *b*-axis. Therefore, we only focus on the comparison between 25DFP and 24DFP, whose $r_e^{SE}$ structures are likely to be more well-determined.

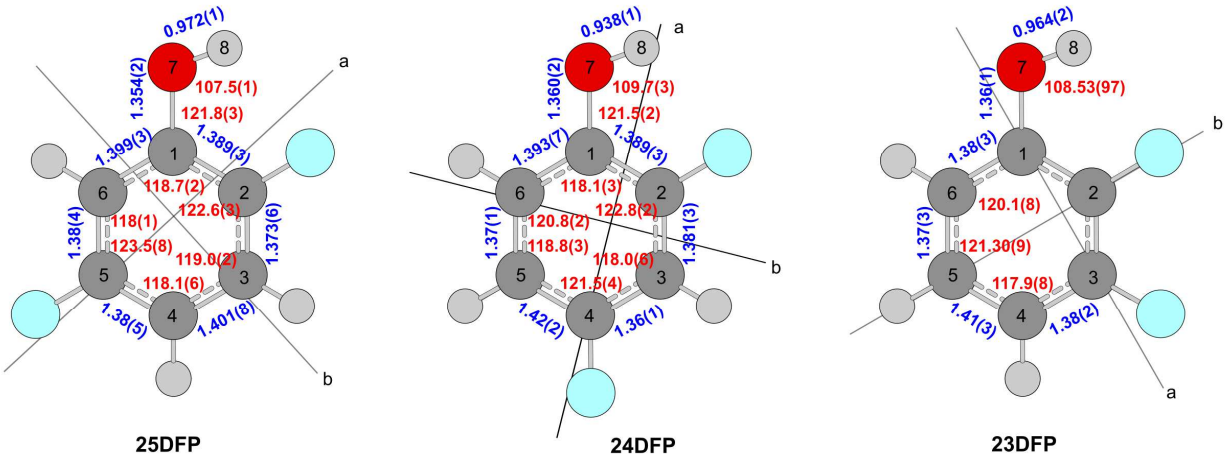


**Figure 4.** Bond lengths (blue, in Å) and bond angles (red, in degrees) of *syn*-25DFP, *syn*-24DFP, and *syn*-23DFP deduced from the $r_{s\rightarrow e}^{SE}$ structure. The statistical uncertainties are 1σ. The *a*- and *b*-principal axes are shown.

An experimental microwave spectroscopic lab often suffers from the limited amount of calculation time, limiting the availability of quantum chemical calculations to be used as a supporting tool. High level coupled-cluster employed in structure determinations of small molecules cannot be reasonably attempted for many molecules of moderate size [56]. Since calculations at the MP2/6-311++G(2d,2p) and B3LYP-D3/aug-cc-pVTZ levels for molecules of the size of 25DFP are often already expensive for an experimental lab, we performed benchmark calculations using many levels of theory including different DFT methods and basis sets to compare the calculation time. The results are summarized in Table S-10 along with the $\Delta B = B_e - B_0$ correction. This table clearly shows that addition of diffuse function significantly increases the calculation time, while $\Delta B$ values are similar. The lowest calculation cost can be achieved at the B3LYP-D3(BJ)/cc-pVDZ level. We thus determined also the $r_s^{SE}$ structure of 25DFP with anharmonic corrections at the B3LYP-D3/cc-pVDZ level. The atom coordinates, bond lengths and bond angles are summarized in Table S-11.

## 5. Discussion and conclusion

Concerning the very rigid phenyl ring, the $r_e^{SE}$ atom coordinates agree well with the $r_e$ structure using the structure determined at the B3LYP-D3/6-311+G(2d,p) level. Anharmonic corrections obtained at the B3LYP-D3/cc-pVDZ level also yield quite satisfactory results with a calculation cost reduced by four times. Therefore, we recommend this level for molecules related to difluorophenol, where computational resources are limited.

The $B_e$ rotational constants of 23DFP, 24DPF, and 25DFP calculated at the MP2/6-311++G(2d,2p) and B3LYP-D3BJ/6-311++G(2d,2p) levels of theory agree well with the experimentally determined constants. In general, the (aug)-cc-pVDZ basis set combines well with DFT method, while (aug)-cc-pVTZ does better with the MP2 method. The best results were achieved at the B3LYP-D3/6-311+G(df,pd) and B3LYP-D3/6-311++G(df,pd) levels of theory for all three isomers. Though not physically meaningful to compare with, using predicted $B_e$ constants from cost-efficient calculations as starting values for experimental $B_0$ constants to guide the assignment of microwave spectra has become an accepted standard, as done in many of our previous studies [57-59]. In a global view, regarding the reasonable cost-performance ratio for anharmonic corrections obtained at the B3LYP-D3/cc-pVDZ calculations and its, at the same time, good performance for geometry optimizations of the three difluorophenol isomers, this level is highly recommended for future investigations on fluorophenol derivatives.

The perfect π-electron delocalization in benzene results in a constant C–C distance of 1.3915 ± 0.0010Å [60] and a constant C–C–C angle of 120° between the six carbon atoms by symmetry. The value of 1.3915 Å is shorter than a C–C single bond of about 1.47 Å but greater than a C–C double bond of 1.35 Å. This $D_{6h}$ symmetry is broken by substitution of the ring. Comparing the $r_e^{SE}$ structure of *syn*-25DFP to the structures of 23DFP and 24DFP, presented in Figure 4, we found that the effect of hydroxyl substitution on the ring geometry in its surrounding is not significant. The C–C bond lengths of the ring at the OH substituted position remains approximately 1.39 Å and the C–C–C angle is close to 120°. On the other hand, the fluorine atoms with their σ-electron withdrawing (–I effect) slightly enlarge the C–C–C angles at the fluoro-substituted positions.

The comparison of semi-experimental equilibrium structures of 25DMF, 23DMF, and 24DMF shows that the O-H bond is shortened when the second fluorine atom is in the *para*

position with respect to the hydroxyl group (0.938 Å in 24DFP compared to 0.972 Å in 25DFP and 0.964 Å in 23DFP, see Figure 5). This is a clear indication that the fluorine atom with its π-electron donating (+M effect) communicates more strongly with the OH group than in the cases where the fluorine atom is at the *meta* position. This also underlines the trend found with respect to the barrier to be overcome in the rotation of the O-H group from the *syn* to the *anti*-conformer (see Figure 2). In this regard, the two *meta*-substituted difluorophenols 23DFP and 25DFP show a higher barrier than the *para*-substituted counterpart 24DFP, which is consistent with the observations for monohalogenated phenols [61]. These two phenomena show again [62] impressively how well the old concept of two- and multiple substitution works and how its correctness can be proven with the aid of simulations and especially experimental investigations.

Furthermore, it is interesting to see how strong the influence of intramolecular dispersion forces is on the formation of the most stable conformation in the gas phase. All three molecules show that the conformer with the hydrogen bonding interaction is dominant, since the intensity of the transitions through the respective *anti* conformers are too small for detection due to the small partition sum under the given molecular jet conditions.

**Acknowledgements**

The authors thank the Land Niedersachsen and the Deutsche Forschungsgemeinschaft (DFG) for funding. This work was supported by the Agence Nationale de la Recherche ANR (project ID ANR-18-CE29-0011) and the European Union (ERC, 101040480-LACRIDO).

**References**


[1] V. M. Bierbaum, V. Le Page, T. P. Snow, Eur. Astron. Soc. Publ. Ser. 46, 427–440 (2011).

[2] B. A. McGuire, R. A. Loomis, A. M. Burkhardt, K. L. K. Lee, C. N. Shingledecker, S. B. Charnley, I. R. Cooke, M. A. Cordiner, E. Herbst, S. Kalenskii, M. A. Siebert, E. R. Willis, C. Xue, A. J. Remijan, M. C. McCarthy, *Science* **371**, 1265−1269 (2021).

[3] B. A. McGuire., A. M. Burkhardt, S. Kalenskii, C. N. Shingledecker, A. J. Remijan, E. Herbst, M. C. McCarthy, *Science* **2018**, *359*, 202.

[4] J. Cernicharo, M. Agúndez, C. Cabezas, B. Tercero, N. Marcelino, J. R. Pardo, and P. de Vicente, *Astron. Astrophys.* **649**, Art. No. L15 (2021).

[5] A. M. Burkhardt, K. L. K. Lee, P. B. Changala, C. N. Shingledecker, I. R. Cooke, R. A. Loomis, H. Wei, S. B. Charnley, E. Herbst, M. C. McCarthy, B. A. McGuire, *Astrophys. J. Lett.* **913**, Art. No. L18 (2021).

[6] H. V. L. Nguyen, J.-U. Grabow, *ChemPhysChem* **21**, 1243-1248 (2020).

[7] X. Wang, Y. Zheng, X. Xu, S. Gao, J. Wang, Q. Gou, *J. Mol. Struct.* **1254**, 132322 (2022).

[8] S. Saxena, S. Panchagnula, M. Sanz, C. Perez, L. Evangelisti, B. H. Pate, *ChemPhysChem* **21**, 2579 (2020).

[9] H. Dreizler, H. D. Rudolph, B. Hartke, *J. Mol. Struct.* **698**, 1 (2004).

[10] A. Melli, F. Tonolo, V. Barone, C. Puzzarini, *J. Phys. Chem. A* **125**, 9904 (2021).

[11] K. E. McCulloh, G. F. Pollnow, *J. Chem. Phys.* **22**, 1144 (1954).

[12] B. Bak, D. Christensen, L. Hansen-Nygaard, E. Tannenbaum, *J. Chem. Phys.* **26**, 134 (1957).

[13] L. Nygaard, I. Bojesen, T. Pedersen, J. Rastrup-Andersen, *J. Mol. Struct.* **2**, 209 (1968).

[14] A. Datta, A. I. Jaman, R. N. Nandi, *J. Mol. Spectrosc.* **114**, 274 (1985).

[15] A. Bell, J. Singer, D. Desmond, O. Mahassneh, J. van Wijngaarden, *J. Mol. Spectrosc.* **331**, 53 (2017).

[16] K. P. R. Nair, S. Herbers, D. A. Dewald, D. Wachsmuth, J.-U. Grabow, *J. Mol. Struct.* **1195**, 479 (2019).

[17] K. P. R. Nair, D. A. Dewald, D. Wachsmuth, J.-U. Grabow, *J. Mol. Spectrosc.* **335**, 23 (2017).

[18] S. Chakrabarti, A. I. Jaman, *J. Mol. Struct.* **642**, 93 (2002).

[19] L. A. Zeoly, F. Coelho, R. A. Cormanich, *J. Phys. Chem. A* **123**, 10072 (2019).

[20] J.-U. Grabow, in Handbook of High Resolution Spectroscopy, Willey, Chichester, pp. 723–799 (2011).

[21] M. Piccardo, E. Penocchio, C. Puzzarini, M. Biczysko, V. Barone, *J. Phys. Chem. A* **119**, 2058 (2015).

[22] H. Ye, M. Mendolicchio, H. Kruse, C. Puzzarini, M. Biczysko, V. Barone, *J. Mol. Struct.* **1211**, 127933 (2020).

[23] C. Puzzarini, V. Barone, *Phys. Chem. Chem. Phys.* **13**, 7189 (2011).

[24] A. Melli, F. Tonolo, V. Barone, C. Puzzarini, *J. Phys. Chem. A* **125**, 9904 (2021).

[25] J. Vazquez, J. F. Stanton, Semiexperimental Equilibrium Structures: Computational Aspects., Taylor and Francis, pp 53-87 (2011).

[26] C. Puzzarini, *Int. J. Quantum. Chem.* **116**, 1513 (2016).

[27] C. Puzzarini, V. Barone, *Acc. Chem. Res.* **51**, 548 (2018).

[28] Z. N. Heim, B. K. Amberger, B. J. Esselman, J. F. Stanton, R. C. Woods, R. J. McMahon, *J. Chem. Phys.* **152**, 104303 (2020).

[29] A. N. Owen, N. P. Sahoo, B. J. Esselman, J. F. Stanton, R. C. Woods, R. J. McMahon, *J. Chem. Phys.* **157**, 034303 (2022).

[30] L. A. Mück, S. Thorwirth, J. Gauss, *J. Mol. Spectrosc.* **311**, 49 (2015).

[31] J. Demaison, N. Vogt, D. N. Ksenafontov, *J. Mol. Struct.* **1206**, 127676 (2020).

[32] J. Demaison, *Mol. Phys.* **105**, 3109 (2007).

[33] C. Dindić, J. Ludovicy, V. Terzi, A. Lüchow, N. Vogt, J. Demaison, H. V. L. Nguyen, *Phys. Chem. Chem. Phys.* **24**, 3804 (2022).

[34] R. S. Ruoff, T. D. Klots, T. Emilsson, H. S. Gutowsky, *J. Chem. Phys.* **93**, 3142 (1990).

[35] C. Møller, M.S. Plesset, *Phys. Rev.* **46**, 618 (1934).

[36] A. D. Becke, *J. Chem. Phys.* **98**, 5648 (1993).

[37] C. Lee, W. Yang, R.G. Paar, *Phys. Rev. B* **37**, 785 (1988).

[38] M. J. Frisch, J. A. Pople, J. S. Binkley, *J. Chem. Phys.* **80**, 3265 (1984).

[39] M. J. Frisch, G. W. Trucks, H. B. Schlegel, G. E. Scuseria, M. A. Robb, J. R. Cheeseman, G. Scalmani, V. Barone, G. A. Petersson, H. Nakatsuji, X. Li, M. Caricato, A. V. Marenich, J.

Bloino, B. G. Janesko, R. Gomperts, B. Mennucci, H. P. Hratchian, J. V. Ortiz, A.F. Izmaylov, J. L. Sonnenberg, D. Williams-Young, F. Ding, F. Lipparini, F. Egidi, J. Goings, B. Peng, A. Petrone, T. Henderson, D. Ranasinghe, V. G. Zakrzewski, J. Gao, N. Rega, G. Zheng, W. Liang, M. Hada, M. Ehara, K. Toyota, R. Fukuda, J. Hasegawa, M. Ishida, T. Nakajima, Y. Honda, O. Kitao, H. Nakai, T. Vreven, K. Throssell, J. A. Montgomery, Jr., J. E. Peralta, F. Ogliaro, M. J. Bearpark, J. J. Heyd, E. N. Brothers, K. N. Kudin, V. N. Staroverov, T. A. Keith, R. Kobayashi, J. Normand, K. Raghavachari, A. P. Rendell, J. C. Burant, S.S. Iyengar, J. Tomasi, M. Cossi, J. M. Millam, M. Klene, C. Adamo, R. Cammi, J. W. Ochterski, R. L. Martin, K. Morokuma, O. Farkas, J. B. Foresman, D. J. Fox, Gaussian 16, Revision B.01, Gaussian Inc., Wallingford CT, 2016.

[40] Y. Zhao, D. G. Truhlar, *Theor. Chem. Acc.* **120**, 215 (2008).

[41] J.-D. Chai, M. Head-Gordon, *Phys. Chem. Chem. Phys.* **10**, 6615 (2008).

[42] C. Adamo, V. Barone, *J. Chem. Phys.* **110**, 6158 (1999).

[43] H. S. Yu, X. He, S. L. Li, D. G. Truhlar, *Chem. Sci.* **7**, 5032 (2016).

[44] T. H. Dunning Jr., *J. Chem. Phys.* **90**, 1007 (1989).

[45] S. Grimme, J. Antony, S. Ehrlich, H. Krieg, *J. Chem. Phys.* **132**, 154104 (2010).

[46] S. Grimme, S. Ehrlich, L. Goerigk, *J. Comput. Chem.* **32**, 1456 (2011).

[47] T. Yanai, D. P. Tew, N. C. Handy, *Chem. Phys. Lett.* **393**, 51 (2004).

[48] J.-U. Grabow, W. Stahl, H. Dreizler, *Rev. Sci. Instrum.* **67**, 4072–4084 (1996).

[49] H. M. Pickett, *J. Mol. Spectrosc.* **148**, 371 (1991).

[50] J. Kraitchman, *Am. J. Phys.* **21**, 17 (1953).

[51] Z. Kisiel, PROSPE-Programs for ROtationalSPEctroscopy, available at http://info.ifpan.edu.pl/~kisiel/prospe.htm.

[52] C. C. Costain, *Trans. Am. Crystallogr. Assoc.* **2**, 157 (1966).

[53] Z. Kisiel, J. Mol. Spectrosc. 218 (2003) 58.

[54] B. J. Esselman, M. A. Zdanovskaia, A. N. Owen, J. F. Stanton, R. C. Woods, R. J. McMahon, *J. Chem. Phys.* **155**, 054302 (2021).

[55] A. N. Owen, M. A. Zdanovskaia, B. J. Esselman, J. F. Stanton, R. C. Woods, R. J. McMahon, *J. Phys. Chem. A* **125**, 7976 (2021).

[56] F. Pawłowski, P. Jørgensen, J. Olsen, F. Hegelund, T. Helgaker, K. L. Bak, J. F. Stanton, J. Chem. Phys. **116**, 6482 (2002).

[57] S. Khemissi, M. Schwell, I. Kleiner, H. V. L. Nguyen, *Phys. Chem. Chem. Phys.* **26**, 402 (2024).

[58] K.J. Koziol, H.E. Hadki, A. Lüchow, N. Vogt, J. Demaison, H. V. L. Nguyen, *Spectrosc. J.* **1**, 49 (2023).

[59] L. W. Sutikdja, H.V.L. Nguyen, D. Jelisavac, W. Stahl, H. Mouhib, *Phys. Chem. Chem. Phys.* **25**, 7688 (2023).

[60] B. J. Esselman, M. A. Zdanovskaia, A. N. Owen, J. F. Stanton, R.C. Woods, R. J. McMahon, *J. Am. Chem. Soc.* **145**, 21785 (2023).

[61] W. Zierkiewicz, D. Michalska, P. Hobza, *Chem. Phys. Lett.* **386**, 95 (2004).

[62] S. Herbers, P. Buschmann, J. Wang, K. G. Lengsfeld, K. P. R. Nair, J.-U. Grabow, *Phys. Chem. Chem. Phys.* **22**, 11490 (2020).